IEEE Open Journal of Vehicular Technology

Received 13 February 2024; accepted 13 March 2024. Date of publication 18 March 2024;
date of current version 5 April 2024. The review of this article was coordinated by Editor Sumei Sun.

Digital Object Identifier 10.1109/OJVT.2024.3378481

Near-Optimal Efficient MIMO Receiver for Miniature UAV-IoT Communications

ANAS SACI [1] (Member, IEEE), ARAFAT AL-DWEIK [2] (Senior Member, IEEE), AND SHIHAB JIMAA [3] (Senior Member, IEEE)

[1]MDA, Montréal, QC H9X 3R2, Canada
[2]6G Research Center, Department of Computer and Communication Engineering, Khalifa University, Abu Dhabi 127788, UAE
[3]Department of Computer and Communication Engineering, Khalifa University, Abu Dhabi 127788, UAE

CORRESPONDING AUTHOR: ARAFAT AL-DWEIK (e-mail: arafat.dweik@ku.ac.ae).

ABSTRACT This article proposes a novel Direct Detection (DD) scheme for multiple-input multiple-output (MIMO) unmanned aerial vehicle (UAV) communications where tedious, slow, and computationally demanding channel state information (CSI) estimation and detection processes are not required. The proposed detection scheme is achieved by exploiting the frequency and/or temporal correlation among the transmitted signals to directly extract the information symbols from the received signals. The results obtained show that the proposed scheme offers a significant advantage of approximately 15 dB performance gain compared to conventional linear detection schemes, even when such schemes are using perfect CSI. Furthermore, the proposed detection algorithm can be efficiently implemented using the Viterbi Algorithm, or its variants, to achieve further complexity reduction.

INDEX TERMS Unmanned aerial vehicle (UAV), fading, diversity, sixth generation (6G), MIMO, Internet of Things (IoT), wireless sensor network (WSN).

I. INTRODUCTION

The last few years have witnessed enormous changes in the role of wireless communications. These changes are mostly caused by the continuous emergence of revolutionary technologies and services related to UAV and IoT applications. For example, UAVs and IoT are currently considered essential for drone-enabled data collection and delivery, smart cities, precision agriculture, and many other applications. Such new wireless services have also changed the distribution of data within the network from a large amount of data at network centers, and hot spots, to massive amounts of small data uniformly distributed over the network coverage area. For such evolution of wireless networks to continue, the 6G of wireless networks is expected to have a highly dynamic architecture, particularly the integration of terrestrial and non-terrestrial networks [1].

In the early days of IoT, applications mainly considered very low data rate transmissions. For example, the SigFox was designed to provide a data rate of 100 bps. Currently, the trend is the demand for higher data rates for IoT applications. For example, LoRaWAN can support up to 50 kbps, and narrowband IoT (NB-IoT) is optimized to support 200 kbps. Furthermore, machine type communications (MTC), which includes the enhanced MTC (eMTC), should be able to support up to 1 Mbps according to the Long Term Evolution (LTE) standard for MTC (LTE-IoT Cat-M1) Release 13, and up to 4 Mbps for Release 14. It is also worth mentioning that the spectral efficiency of LTE-MTC is about 0.8 bit/sec/Hz [2]. When considering the massive number of devices that will be connected, a higher spectral efficiency will be indispensable in the near future. In contemporary IoT applications, sensory data will be collected from various locations and sensors using UAVs [3], [4], [5], and then sent to remote cloud-based decision centers for data fusion and action decision [6], [7]. Consequently, the UAV will be the hub between the sensors and the fusion center, and hence should not be the bottleneck in the transmission chain. As a key enabler for spectral efficiency and reliability enhancement techniques, diversity technologies are playing a major role in most recent wireless standards [8]. Such technologies can be realized in various transmit/receive diversity schemes, which include MIMO systems [9], massive-multiple-input multiple-output

(mMIMO) [10], [11], and the emerging intelligent reflecting surface (IRS) techniques [12].

Theoretically, a MIMO system can provide a Q-fold increase in transmission capacity, where Q is the rank of the MIMO channel matrix, and maximum capacity can be achieved when the MIMO channel matrix is a full-rank matrix [13]. As technology continues to evolve and advance, mMIMO is expected to be one of the main pillars of the upcoming 6G standard to enable ultra-reliable low-latency communication (URLLC) services [14], [15], [16], [17]. Although mMIMO has been proposed in the literature for IoT applications, the multiple antennas are typically installed at the base station (BS) side, multi user (MU)-MIMO, because IoT nodes cannot generally support a large number of antennas [18], [19], and the MIMO detection process requires heavy computations and CSI estimation at both the BS and IoT nodes [10], [11]. The main goal of mMIMO in such applications is to steer the antenna beam towards a particular node that typically supports single or double antennas. However, mMIMO can be installed only on large BSs, which is not suitable for UAV-ground applications where usually a private gateway, wireless access point (WAP), or cluster-head (CHD) is used to provide wireless access to the UAVs, such a configuration is very popular in fifth generation (5G) where it is commonly referred to as private networks. The same argument applies to UAV-to-UAV communications. In such scenarios, the nodes have constraints in terms of size, cost, and computational power. Thus, it can support only a single or a couple of antennas [20].

The private communications sector has a wide range of transceiver designs to support UAV communications. Due to the size and computational power limitations, such systems typically support 2×2 MIMO. For example, the THPR1009-D03 high-power radio supports 2×2 MIMO in the C-band with a frequency of 4.4–4.7 GHz [21]. Although the THPR1009-D03 size is generally large, $17.78 \times 16.51 \times 3.93$ cm, installing more than 2 antennas on the device is challenging. There are several other systems, even with much smaller sizes, such as the RFD900 A autopilot flight controller [22]. The dimensions of the RFD900 A are $3.2 \times 5.3 \times 0.95$ cm. Therefore, installing more than two antennas is infeasible, particularly at low frequencies, due to the severe channel correlation that may result. The 4×4 MIMO can be found in some high-end UAV receivers [23], which can support both spatial multiplexing and space-time block codes (STBC).

A. RELATED WORK

In the literature, several articles have considered the complexity reduction problem of MIMO detectors. Among several techniques, Sphere decoding is considered one of the well-established approaches [24], [25], [26], [27], [28], [29]. Stochastic sampling is another widely considered approach as reported in [30] and the references listed therein, particularly [28], [29], [31], [32], [33], [34], [35], [36]. Nevertheless, the complexity of MIMO detectors remains of great concern and still attracts significant attention. For example, For example, Hijazi et al. proposed a near-optimal MIMO detector by combining ordered successive interference cancellation (SIC) and maximum likelihood detector (MLD). The proposed ordered SIC shows a near-optimal performance at lower complexity compared to other detectors such as the sphere detector. However, the ordered SIC detector does not reduce signaling requirements or reduce the need for channel estimation and data detection. Hama and Ochiai [37] analyzed the performance of the low-complexity matched filter detector for MIMO and derived exact bit error rate (BER) expressions. However, the matched filter offers poor BER performance. Lin et al. [38] proposed to eliminate the need for CSI by using frequency shift keying and energy detection with vertical-Bell laboratories layered space-time (V-BLAST). However, the BER performance of the proposed linear detector system is significantly worse than that of the MLD as well as the coherent detectors. To obtain diversity gain without completely using space diversity, Iraqi and Al-Dweik [9] proposed a smart orthogonal frequency division multiplexing (OFDM) in which certain subcarriers are shared by multiple data streams. Although smart OFDM managed to provide significant diversity gain, it does not provide a capacity improvement. Moreover, the achieved diversity gain depends on the channel frequency selectivity and may vanish in flat-fading channels.

As can be noted from the surveyed literature and the literature listed therein, and to the best of the authors' knowledge, there is no work in the literature that considers the MIMO detection process holistically, that is, channel estimation, pilot use reduction, equalization, and symbol detection. Therefore, the aim of this work is to propose a novel scheme that can deal with multiple disjoint processes jointly.

B. MOTIVATION AND CONTRIBUTION

As can be noted from the aforementioned discussion, integrating MIMO with IoT and UAVs may face challenges in terms of computational complexity, processing power, spectral efficiency, and communication reliability. While spatial multiplexing can improve the link spectral efficiency, the use of linear receivers eliminates the diversity gain that can be obtained using MLD, which is usually avoided due to its high complexity. Therefore, capitalizing on our work in [39], we propose in this work a novel DD-MIMO receiver with the following features:

- Does not require CSI estimation, which is a critical process in all conventional MIMO detectors.
- Channel matrix inversion, or pseudo-inversion, and equalization operations are not required.
- Does not require single-layer (SL)-MLD.
- Requires less signaling overhead because antenna muting is not required.
- It has low complexity because it can be realized using the Viterbi Algorithm or its variants.
- Offers a significant BER improvement because it partially maintains the diversity gain.

C. PAPER ORGANIZATION

The rest of the paper is organized as follows. Section II presents the V-BLAST MIMO system and channel models. Section III describes the proposed DD system. Section IV discusses the numerical results, and finally, Section V concludes the article and highlights some open research problems and future work.

II. V-BLAST MIMO SYSTEM AND CHANNEL MODELS

This work considers the V-BLAST MIMO configuration. Therefore, the main data stream at the transmitter is split into N_T layers each of which is assigned to a specific antenna. The N_T data layers are transmitted simultaneously using the N_T antennas. The transmitted data vector is denoted as $\mathbf{x} = [x_1, x_2, \ldots, x_{N_T}]$. To enable layer separation at the receiver side, the number of receiving antennas N_R should satisfy the condition $N_R \geq N_T$. Extracting the data symbols coherently at the receiver requires accurate knowledge of the CSI between the N_T transmit and N_R receive antennas, which is typically represented by the matrix $\mathbf{H} \in \mathbb{C}^{N_R \times N_T}$. Therefore, a certain channel estimation technique should be used to estimate $\mathbf{H}$. In wireless communications standards such as fourth generation (4G) and 5G, the channel estimation process is performed by inserting pilot symbols as part of the transmitted resource block. For completeness, the following subsection briefly introduces the channel estimation process in the 3rd Generation Partnership Project (3GPP) standards.

A. PILOT SIGNALING IN CURRENT 3GPP STANDARDS

In the LTE and fifth generation new radio (5G NR), coherent detection is performed through CSI estimation at the receiver side. This is achieved by adding known reference symbols, pilots, to the OFDM time-frequency grid to be used for the CSI estimation. Such reference symbols are distributed in each resource block with a particular spacing so that the two-dimensional Nyquist sampling theorem is satisfied. Interpolation can be used to calculate CSI in the data subcarriers [39]. For MIMO systems, each antenna is assigned its own reference signals. Moreover, when the reference signals for a particular antenna are transmitted, all other antennas should be muted to avoid pilot contamination. The muting process is equivalent to inserting a null symbol, i.e., modulating the subcarrier with a symbol that has zero amplitude. Fig. 1 shows the resource grids for a 2×2 MIMO showing the reference and null symbols. As can be noted from the figure, the 12 subcarriers in a given OFDM symbol have two pilot symbols located at subcarriers 1 and 7. Therefore, subcarriers $\{2, 3, \ldots, 6\}$ are enclosed by two pilots, thus, this scenario is denoted as the double-sided configuration. For subcarriers $\{8, 9, \ldots, 12\}$, they are enclosed only by one pilot at subcarrier 7, and hence this scenario is denoted as the single-sided configuration. Moreover, the pilot symbols can be transmitted with various power levels where the process is called power boosting [41], and power boosting factor is denoted by $\beta \in \{0, 3, 6\}$ dB.

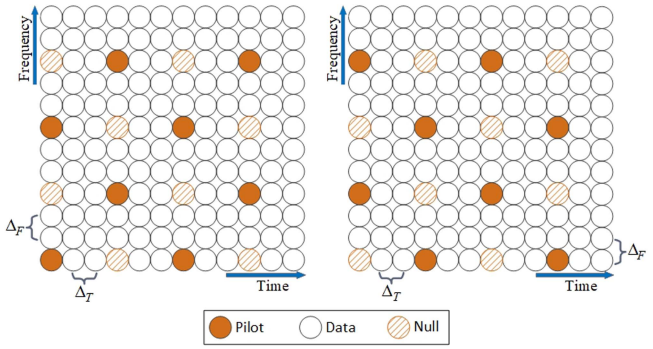

FIGURE 1. LTE resource blocks for a 2 × 2 MIMO transmission mode [40].

Given that antenna j has transmitted a pilot symbol P_j, the received signal at receiver i can be expressed as

$$r_i = h_{i,j} P_j + z_i. \tag{1}$$

Accordingly, the least square estimation (LSE) can be used such that the estimated channel can be written as

$$\hat{h}_{i,j} = \frac{r_i}{P_j} = h_{i,j} + \tilde{z}_i \tag{2}$$

where $\mathrm{E}[|P_j|^2] = 1$, $\mathrm{E}[\cdot]$ denotes the statistical expectation, $\tilde{z}_i = \frac{z_i}{P_j}$, $\{z_i, \tilde{z}_i\} \sim \mathcal{CN}(0, \sigma_z^2)$. Once the channel estimates are obtained at the pilot subcarriers, various interpolation techniques can be used to compute the channels frequency-response at all other subcarriers [42]. As can be noted, the channel estimation process for MIMO systems deteriorates the spectral efficiency of the system in multiple ways. First, the pilot symbols themselves do not carry information. Second, when a pilot symbol is transmitted, all other transmit antennas are not allowed to use the channel, and finally, the process has to be performed for each antenna individually.

For UAV communications, the transmission process is usually performed while hovering, or moving at low speeds, above the ground nodes at relatively low altitudes [43]. Therefore, the UAV-ground channel will suffer small-scale fading due to the reflected signals from ground objects. Moreover, UAV wobbling and mobility will introduce Doppler shifts. However, the statistical properties of the channel remain stationary [44]. In this work, the channel between any two antennas at the transmitter and receiver is modeled as a Rayleigh fading to capture the multipath reflections from ground objects. Moreover, the UAV mobility is considered by introducing a temporal envelope variation that follows the Jakes' Doppler spectrum model [45], [46].

B. OVERVIEW OF MIMO DECODING SCHEMES

Once the CSI of a MIMO system is estimated, a certain detector is used to extract the data symbols by removing the channel effect, inter-symbol interference (ISI), and reducing the effect of additive white Gaussian noise (AWGN) at the input of the receiving antennas. In practice, computational complexity

is considered a key design parameter in several communications systems applications. Accordingly, linear equalizers are typically used to eliminate/reduce the noise and extract the information symbols in MIMO systems. The main MIMO detection schemes are the optimum MLD, zero-forcing equalizer (ZFE), and minimum mean square error equalizer (MMSEE), which can be described as follows:

1) MLD

The MLD can be expressed as

$$\hat{\mathbf{x}} = \arg\min_{\underline{\mathbf{x}} \in \mathbb{X}} \left\| \mathbf{r} - \hat{\mathbf{H}}\underline{\mathbf{x}} \right\|^2 \tag{3}$$

where $\mathbf{r} = [r_1, r_2, \ldots, r_{N_R}]$, $\mathbb{X}$ is the set of all possible combinations of the data vector $\mathbf{x} = [x_1, x_2, \ldots, x_{N_T}]$, $\underline{\mathbf{x}}$ are the trial values of $\mathbf{x}$, x_i is the modulated data symbol, and $\| \cdot \|$ is the Euclidean norm.

2) ZFE

Eliminates the interference from all signals using the Moore–Penrose inverse weighting matrix $\mathbf{W}$,

$$\mathbf{W} = \left(\hat{\mathbf{H}}^{\dagger}\hat{\mathbf{H}}\right)^{-1}\hat{\mathbf{H}}^{\dagger}. \tag{4}$$

where $[\cdot]^{\dagger}$ denotes the hermitian transpose operation. Therefore, the equalized symbols can be expressed as

$$\mathbf{s} = \mathbf{W}\mathbf{r} = \mathbf{x} + \mathbf{n} \tag{5}$$

where $\mathbf{n} = (\hat{\mathbf{H}}^{\dagger}\hat{\mathbf{H}})^{-1}\hat{\mathbf{H}}^{\dagger}\mathbf{z}$. Once the equalized vector $\mathbf{s}$ is obtained, its symbols are applied to a SL-MLD to generate the estimated symbols vector $\hat{\mathbf{x}}$.

3) MMSEE

This equalizer is used to maximize the signal to interference and noise ratio (SINR), where its weighting matrix $\mathbf{W}$ is given by

$$\mathbf{W} = \left(\hat{\mathbf{H}}^{\dagger}\hat{\mathbf{H}} + \sigma_z^2\mathbf{I}\right)^{-1}\hat{\mathbf{H}}^{\dagger} \tag{6}$$

where $\mathbf{I}$ is an $N_T \times N_T$ identity matrix. As seen from (6), the MMSEE equalizer requires the knowledge of the noise variance σ_z^2. Then, the equalized vector can be written as

$$\mathbf{s} = \mathbf{W}\mathbf{r} = \mathbf{x} + \boldsymbol{\zeta} + \mathbf{n} \tag{7}$$

where $\boldsymbol{\zeta}$ is the ISI and $\mathbf{n} = (\hat{\mathbf{H}}^{\dagger}\hat{\mathbf{H}} + \sigma_z^2\mathbf{I})^{-1}\hat{\mathbf{H}}^{\dagger}\mathbf{z}$. The ISI term is introduced because $(\hat{\mathbf{H}}^{\dagger}\hat{\mathbf{H}} + \sigma_z^2\mathbf{I})^{-1}\hat{\mathbf{H}}^{\dagger} \neq \mathbf{H}^{-1}$. Nevertheless, the MMSEE equalizer reduces the noise amplification phenomenon, which has more impact than $\boldsymbol{\zeta}$ on the error performance of the MIMO system [47]. Once the equalized vector $\mathbf{s} = [s_1, s_2, \ldots, s_N]$ is obtained, it can be applied to the SL-MLD.

Although the ZFE and MMSEE have less complexity than MLD, they still have considerable complexity due to the channel estimation and inversion processes, and the noise variance estimation for the MMSEE. Moreover, the ZFE and MMSEE cause significant performance degradation as compared to the MLD where the diversity gain vanishes. Furthermore, channel estimation errors can degrade the performance of all CSI-based MIMO detectors.

III. PROPOSED DIRECT DETECTION OF MIMO SIGNALS

The small time, frequency, or space separation among adjacent and subsequent transmitted data blocks creates frequency, spatial, and temporal correlation at the receiver side. Spatial correlation rises when different multipath components have strong spatial signatures in the sense that certain average signal gains are received from a particular spatial direction. Specifically, spatial correlation means a correlation between the received average signal gain and the angle of arrival. Temporal correlation, on the other hand, results from slowly varying characteristics of different fading channels [48]. Frequency correlation depends on the channel frequency selectivity, and the maximum correlation is achieved in flat fading channels [9].

The spatial correlation phenomena become apparent in wireless networks when operating in ultra-dense urban areas. In such scenarios, there will be many physical obstacles that force transmitted signals through a limited number of propagation paths. Furthermore, working in ultra-high frequencies (UHF) limits the number of communications paths and enforces beams of radiation through predetermined spatial routes. For MIMO systems, spatial correlation can reduce the diversity gain obtained using the MIMO configuration. The spatial correlation can be mitigated by increasing the distance between the antennas beyond half of the carrier signal wavelength. However, for WSNs, the sensors have very small areas, which limits the number of antennas that can be used.

The temporal correlation is inversely proportional to the Doppler shifts of the communications link [45]. Accordingly, the temporal correlation of transmitted signals reaches its maximum with fixed transmitter/receiver nodes and starts decreasing when the speed of either one of the communicating devices increases. As such, temporal correlation is expected to be high for several IoT and WSN applications where the nodes are typically stationary or moving slowly. Fig. 2 shows the channel gain for a 2×2 MIMO over a period of 50μ sec. As can be noted from the figure, the channels' temporal correlation is high even for such high speeds of 200 km/h. The temporal correlation is usually characterized using the coherence time of the channel. On the other hand, the frequency correlation depends on the relation between the transmission symbol rate and the maximum delay spread of the channel, which can be characterized using the coherence bandwidth of the channel. Generally speaking, the coherence bandwidth is in the order of several hundreds of kHz, which implies that the channel is generally flat when the symbol rate is in the order of several hundreds of kilo symbols per second. Consequently, the channel for several IoT and WSN applications can be considered flat.

If not considered appropriately, channel correlation may cause severe degradation to the diversity and coding gains, and thus, the MIMO system capacity [45]. Therefore, this

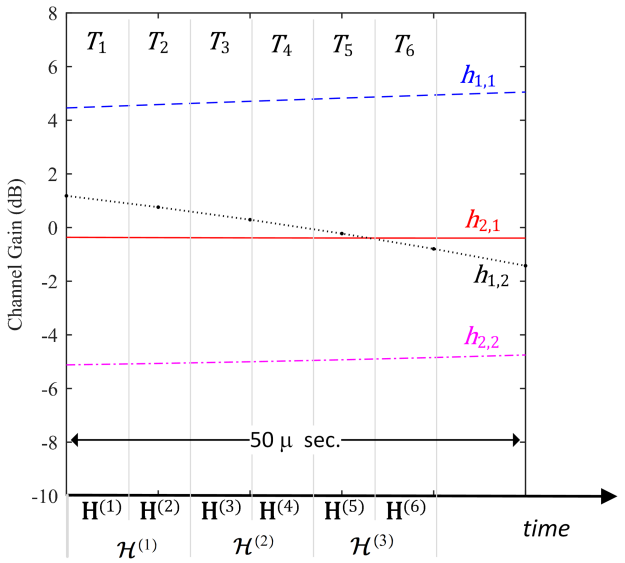

FIGURE 2. Example of channel correlation assumption where $K = 3$ and $L = 2$, speed 200 km/h and frequency is 6 GHz, Doppler frequency is about 1100 Hz. Given that the symbol rate is 200 × 10^3 symbol/sec., the 50 μ s corresponds to 10 symbols.

Algorithm 1 : DD of MIMO Signals.

Input: $K, L, \mathbf{r}^{(1)}, \ldots, \mathbf{r}^{(LK)}, \mathbb{X}$.
Initialize: Compute $\mathbb{X}^{-1}$, $\mathbf{R}^{(1)} = \mathbf{0}_{N_T \times KL}$
for $k = 1 : K$ **do** ▷ # of signaling blocks
  for $l = 1 : L$ **do** ▷ # of signaling periods
    $\mathbf{R}^{(k)}[:, l] = \mathbf{r}^{(l)}$ ▷ Buffering
  end for
end for
Solve (15) to find $\hat{\mathbf{X}}$.
Output: $\hat{\mathbf{X}}$

work proposes a novel DD scheme where the channel correlation is exploited to reduce the complexity and improve the performance of the MIMO detection process. It is worth noting that the DD in this work is different from the DD that is commonly used in optical communications, which is based on detecting the modulated optical power [49]. The proposed DD is still classified as coherent, however, it does not follow the typical processes used in conventional coherent detection. To illustrate the concept of the proposed MIMO direct detection scheme, consider a MIMO system with N_T transmit and N_R receive antennas, that support V-BLAST. In this work we consider the downlink transmission from a miniature UAV to multiple IoT/WSN terrestrial devices. Therefore, the received signal at the ith receiving antenna for a given IoT device can be written as

$$r_i = h_{i,1}x_1 + h_{i,2}x_2 + \cdots + h_{i,N_T}x_{N_T} + z_i, \quad i \in \{1, 2, \ldots, N_R\}. \tag{8}$$

In matrix notation, the received vector for the N_R receive antennas for the kth signaling period is given by,

$$\mathbf{r}^{(k)} = \mathbf{H}^{(k)}\mathbf{x}^{(k)} + \mathbf{z}^{(k)} = \begin{bmatrix} h_{1,1}^{(k)} & h_{1,2}^{(k)} & \cdots & h_{1,N_T}^{(k)} \\ h_{2,1}^{(k)} & h_{2,2}^{(k)} & \cdots & h_{2,N_T}^{(k)} \\ \vdots & \vdots & \ddots & \vdots \\ h_{N_R,1}^{(k)} & h_{N_R,2}^{(k)} & \cdots & h_{N_R,N_T}^{(k)} \end{bmatrix} \begin{bmatrix} x_1^{(k)} \\ x_2^{(k)} \\ \vdots \\ x_{N_T}^{(k)} \end{bmatrix} + \begin{bmatrix} z_1^{(k)} \\ z_2^{(k)} \\ \vdots \\ z_{N_R}^{(k)} \end{bmatrix}. \tag{9}$$

In the V-BLAST transmission mode, a unique information symbol is transmitted from each transmit antenna. Therefore, the MIMO transmitter at the UAV requires N_T radio frequency (RF) chains, each responsible for the baseband processing and modulation of a single information block for a particular IoT receiving device. Buffering the signals for $L \geq N_T$ signaling periods gives

$$\mathbf{R}^{(1)} = \left[\mathbf{r}^{(1)}, \mathbf{r}^{(2)}, \ldots, \mathbf{r}^{(L)}\right] = \left[\mathbf{H}^{(1)}\mathbf{x}^{(1)}, \mathbf{H}^{(2)}\mathbf{x}^{(2)}, \ldots, \mathbf{H}^{(L)}\mathbf{x}^{(L)}\right] + \mathbf{Z}^{(1)} \tag{10}$$

where $\mathbf{Z}^{(1)} \in \mathbb{C}^{N_R \times L}$ is the AWGN matrix. In slow and block fading channels, it can be assumed that

$$\mathbf{H}^{(1)} \approx \mathbf{H}^{(2)} \approx \mathbf{H}^{(L)} \triangleq \mathcal{H}^{(1)}. \tag{11}$$

Accordingly, we can rewrite (10) as

$$\mathbf{R}^{(1)} = \mathcal{H}^{(1)}\left[\mathbf{x}^{(1)}, \mathbf{x}^{(2)}, \ldots, \mathbf{x}^{(L)}\right] + \mathbf{Z}^{(1)} = \mathcal{H}^{(1)}\mathbf{X}^{(1)} + \mathbf{Z}^{(1)}. \tag{12}$$

If the same process is applied to K blocks each of which has L symbol periods, the kth received block can be expressed as

$$\mathbf{R}^{(k)} = \mathcal{H}^{(k)}\mathbf{X}^{(k)} + \mathbf{Z}^{(k)}, \tag{13}$$

where $k = 1, 2, \ldots, K$. However, in slow fading channels, the matrices $\mathcal{H}^{(k)}$ and $\mathcal{H}^{(k+1)}$ are highly correlated, and it can be assumed that $\mathcal{H}^{(k)} \approx \mathcal{H}^{(k+1)}$. Given that that $\mathbf{X}^{(k)}$ and $\mathbf{X}^{(k+1)}$ are invertible matrices, [R1,6]then by ignoring $\mathbf{Z}$ and assuming that $\mathbf{X}^{(k)}$ and $\mathbf{X}^{(k+1)}$ are known we can formulate the following relation,

$$\begin{aligned} \mathbf{R}^{(k)}\check{\mathbf{X}}^{(k)} - \mathbf{R}^{(k+1)}\check{\mathbf{X}}^{(k+1)} &= \mathcal{H}^{(k)}\mathbf{X}^{(k)}\check{\mathbf{X}}^{(k)} - \mathcal{H}^{(k+1)} \\ &\quad \times \mathbf{X}^{(k+1)}\check{\mathbf{X}}^{(k+1)} \\ &= \mathcal{H}^{(k)} - \mathcal{H}^{(k+1)} \\ &\approx \mathbf{0}_{N_R \times N_T} \end{aligned} \tag{14}$$

where $\check{\mathbf{X}} = \mathbf{X}^{-1}$. It should be noted that the assumption of high temporal correlation is particularly valid for IoT/WSNs because the UAV in the data collection phase is grabbing over the device or moving at low speeds. Similarly, the sensing nodes, the cluster head, or the IoT gateway are typically static or moving at relatively low speeds.

Based on (14), the received information signals during each $K \times L$signaling periods, i.e, $\mathbf{X}^{(1)}, \ldots, \mathbf{X}^{(K)}$ can be estimated

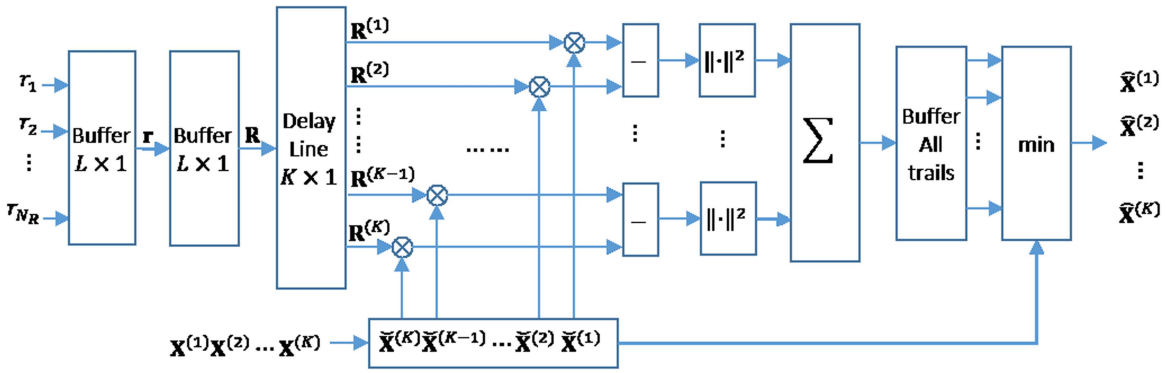

FIGURE 3. Proposed DD block diagram.

using the following detection rule,

$$\left[\hat{\mathbf{X}}^{(1)},\ldots,\hat{\mathbf{X}}^{(K)}\right] = \arg \min_{\left[\underline{\mathbf{X}}^{(1)},\ldots,\underline{\mathbf{X}}^{(K)}\right]} \sum_{k=1}^{K-1} \left\| \mathbf{R}^{(k)}\underline{\mathbf{X}}^{(k)} - \mathbf{R}^{(k+1)}\underline{\mathbf{X}}^{(k+1)} \right\|^2. \quad (15)$$

Therefore, the estimated data matrices can be obtained by using an inverse trial matrices $\underline{\mathbf{X}}$, and then select the set of matrices that minimizes (14).

Evidently, the solution of the proposed MIMO symbol detection problem in (15) does not require any estimation for the CSI matrices. Moreover, it avoids the highly-complex channel matrix inversion process at each time slot, as in the case of ZFE and MMSEE. Because the trial matrices $\underline{\mathbf{X}}$ are independent of $\mathbf{R}$, their calculation is conducted only once at the pre-configuration stage of the detector, and then they will be called from a certain lookup table during the detection process. **Algorithm 1** and Fig. 3 further illustrate the consecutive steps of the proposed DD for MIMO systems. In step 2, matrix $\mathbf{R}^{(1)} \in 0^{N_T \times KL}$ is initiated, and then it is partitioned and populated recursively to construct the received signal matrices $\mathbf{R}^{(1)}, \mathbf{R}^{(2)}, \ldots, \mathbf{R}^{(K)}$ in steps 3 to 7. In each loop iteration, the received vector $\mathbf{r}$ is saved to $\mathbf{R}$, which is partitioned into K equal matrices. Once the received K matrices are ready, they are used to obtain the estimated data matrix $\hat{\mathbf{X}}$ in step 8. The solution can be performed using (15) or using the Viterbi detector.

Although the DD functionality is described in the time domain, the DD can also be applied in the frequency domain, but with minor modifications. In the frequency domain, the system buffers the signals for $L \geq N_T$ subcarriers, then (10) is constructed by buffering the adjacent subcarriers, and the remaining part of the system design is obtained by replacing the time indices with the subcarrier indices. In such cases, the channel frequency selectivity across adjacent subcarriers should be roughly equal, which is mostly the case in flat and moderate frequency-selective (FS) channels. The adoption of the time or frequency domain depends on the targeted application. If channel variation in the time domain is expected to be greater than in the frequency domain, then it would be better to adopt the frequency domain realization in the system. The variations can be measured using the correlation factor in the time and frequency domains, which can be used to decide which mode is used.

A. PRACTICAL DESIGN ASPECTS OF THE DD SCHEME

It is worth noting that the detection process described by the objective function described in (15) may have the same solution for different values of $\mathbf{X}^{(k)}$ and $\mathbf{X}^{(k+1)}$. Furthermore, the matrix $\mathbf{X}$ might be singular, that is, it does not have an inverse, as in the case where all elements of the trial matrix are identical, which implies that (15) cannot be solved. To overcome this problem and avoid such scenarios, we recall that most commercial standards such as LTE and 5G NR use reference symbols, pilots, for channel estimation. Therefore, the pilot symbols can be exploited to solve the singularity problem by selecting the pilot symbol alphabet to be different from the data symbol alphabet. Another potential solution can be achieved by changing the symbols' alphabet versus the signaling period. As an example, for 2×2 V-BLAST MIMO with binary phase-shift keying (BPSK), the symbol alphabet in a given signaling period can be $\{1, -1\}$ while in the next period it can be $\{j, -j\}$, where $j = \sqrt{-1}$.

B. COMPLEXITY ANALYSIS

Given that the number of data trial matrices is K, $\mathbf{X}^{(1)}, \ldots, \mathbf{X}^{(K)}$, the number of data symbols in each matrix is $\mathcal{Q}$ with modulation order M, then the number of times the objective function in (15) should be evaluated is $K^{\mathcal{Q}M}$. Because the size of matrix $\mathbf{R}$ and matrix $\mathbf{X}$ is generally small, the computational complexity of the objective function core is reasonable. However, for large values of K, the complexity becomes quite high. Therefore, low complexity approaches have to be designed for the practical implementation of the proposed DD scheme. A significant reduction in complexity can be achieved in solving the problem in (15) by using the fact that each term in (15) appears twice in two consecutive sums of k. Therefore, the Viterbi algorithm can detect the matrices $\mathbf{X}^{(1)} \ldots \mathbf{X}^{(K)}$ sequentially. Fig. 4 presents the sequential detection process for a system with $\mathcal{Q} = 3$ and BPSK. The figure is labeled with trial data matrices $\mathbf{X}^{(i)} \in \{\mathbf{X}_1, \mathbf{X}_2, \ldots, \mathbf{X}_8\}$,

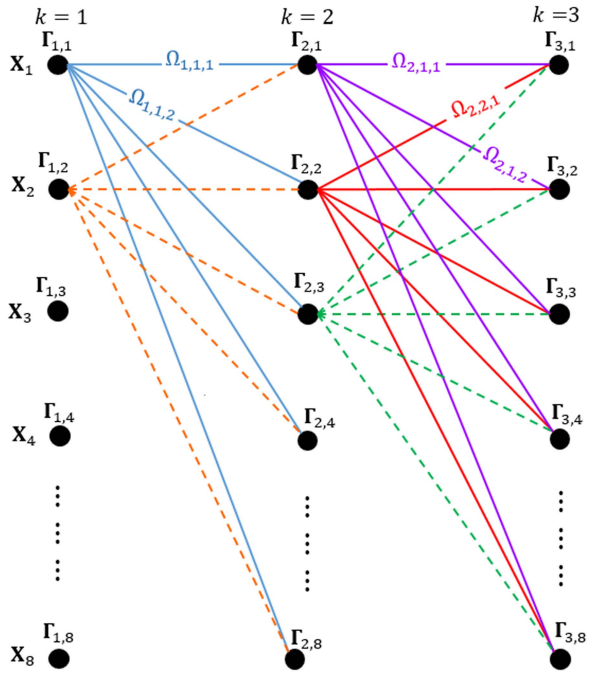

FIGURE 4. Proposed system using sequential detection, $K = 3$ and $L = 2$, and $M = 2$.

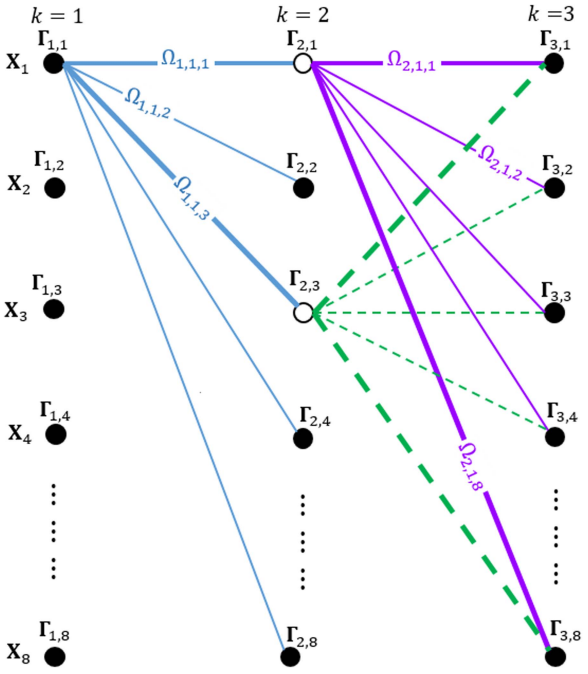

FIGURE 5. Proposed system using sequential detection with node elimination, $K = 3$ and $L = 2$, and $M = 2$.

the branch metrics $\Omega_{k,m,n}$, and the path metrics $\mathbf{\Gamma}_{k,m}$. The branch metrics are defined as

$$\left\| \mathbf{R}^{(k)} \check{\mathbf{X}}_m - \mathbf{R}^{(k+1)} \check{\mathbf{X}}_n \right\|^2 \triangleq \Omega_{k,m,n}. \tag{16}$$

At each connection node, the path metric $\Gamma_{k,m,n}$ is computed as the sum of all branch metrics on the path leading to that node. For example, the path metrics $\mathbf{\Gamma}_{1,1}$, $\mathbf{\Gamma}_{2,1}$ and $\mathbf{\Gamma}_{3,1}$, in the figure are given by

$$\mathbf{\Gamma}_{1,1} = \begin{bmatrix} 0 \\ 0 \\ \vdots \\ 0 \end{bmatrix}, \mathbf{\Gamma}_{2,1} = \begin{bmatrix} \Omega_{1,1,1} \\ \Omega_{1,2,1} \\ \vdots \\ \Omega_{1,8,1} \end{bmatrix}, \mathbf{\Gamma}_{3,1} = \begin{bmatrix} \Gamma_{2,1,1} + \Omega_{2,1,1} \\ \Gamma_{2,2,1} + \Omega_{2,2,1} \\ \vdots \\ \Gamma_{2,8,1} + \Omega_{2,8,1} \end{bmatrix}.$$

Each connected node in the figure has 8 different links, resulting in 8 path metrics at each node. Similar to the typical Viterbi algorithm, the paths' metrics at each node for the converging paths are compared, and the path with minimum value is considered the survivor while the remaining paths are discarded. As can be depicted from the figure, proceeding from one state to the next requires computing (15) only 8 times, which noticeably requires less computational power compared to performing 64 operations at each stage in a non-Viterbi solution.

In conventional V-BLAST MIMO receivers, the CSI should be estimated and then used to equalize the received signal. And finally, the equalized symbols are sent to a bank of SL-MLDs to find the most probable data symbols. Typically, equalization in MIMO systems is performed through ZFE or MMSEE. In ZFE, the effect of the MIMO channel is removed directly by multiplying the received signal by the inverse, or pseudoinverse, of the MIMO CSI matrix. In MMSEE, on the other hand, the received signal is pre-multiplied by the MIMO channel matrix shifted by approximate values of the covariance matrix of the AWGN. Therefore, both ZFE and MMSEE signal detection schemes suffer from critical complexity issues related to the requirement for accurate CSI estimates at each signaling period, which requires complex division and interpolation operations. Moreover, the channel matrix inversion process generally requires a large number of mathematical operations. The effect of these issues becomes more critical as the number of transmit/receive antennas of the MIMO system increases. The MLD complexity is generally higher than ZFE and MMSEE [47].

Although the use of the Viterbi algorithm can reduce the proposed system complexity, the number of branches at each transition is equal to the total number of states the trellis. To reduce the complexity of the Viterbi Algorithm, various algorithms have been proposed in the literature to limit the number of branches going out of each state [50], [51]. Fig. 5 shows an example for the K-best branches approach where $K = 2$. The selected branches in the figure are the ones with the lowest branch metrics, which are represented by the thick lines. As can be seen in the figure, the number of branches and paths at each state is significantly reduced. The results in [50] show that the performance degradation for $K \geq 4$ is negligible.

IV. NUMERICAL RESULTS

To evaluate the performance of the proposed DD scheme, the LTE standard is used as the basis for an OFDM system with a

sampling frequency of $f = 3.836$ MHz, $N = 512$ subcarriers and $N_{CP} = 64$ cyclic prefix samples. This setup is adopted because the narrowband IoT (NB-IoT) standard generally follows the LTE physical layer structure. Single and double-sided pilot configurations are used with pilot power boost, $\beta = 0$ and 3 dB. The performance of the DD is benchmarked against the optimal MLD, ZFE, and MMSEE. The performance of the three benchmarking schemes is evaluated with perfect and imperfect CSI. For the latter scenario, the channel matrix $\hat{\mathbf{H}}$ is estimated at the pilot positions using a LSE estimator and then linear or spline interpolation is used to estimate the CSI values for the data subcarriers. Although the proposed scheme is generally applicable to various MIMO configurations with a wide range of N_T and N_R values, the numerical results in this work consider the 2×2 V-BLAST configuration, since it is highly suitable for IoT, WSNs, and UAV applications [21], [22]. Generating results for other MIMO configurations is straightforward. In fact, the more antennas involved in the communications setup, the more performance gain can be acquired using the proposed DD scheme. The DD and all other systems are implemented in the frequency domain.

To evaluate the DD system performance under various operating conditions, two different channel models are considered. The first corresponds to a flat Rayleigh fading channel where all subcarriers undergo the same fading effects, which is typically used to model narrow-band communications. The second channel model corresponds to FS multipath fading channel, which is typically used to model broadband transmission. The adopted FS channel follows the typical urban (TU) fading model, which represents a moderate 6-taps FS channel with normalized delays of 0, 2, 3, 9, 13, and 29 samples. The multipath components are generated as complex zero-mean Gaussian random variables where the average gain for each tap is -3, 0, -2, -6, -8, and -10 dB. In each simulation run, 10×10^6 OFDM symbols are generated. The 2×2 MIMO channels are considered mutually independent. For all scenarios considered, the total power allocated to all pilot symbols is equal to make a fair comparison among different scenarios. The configurations of the pilot symbols used for the conventional MIMO follow the LTE resource block [40] depicted in Fig. 1. For the proposed detection scheme, two different designs are considered, the single and double-sided pilot cases. For the single-sided case, the null subcarriers are replaced by regular data symbols, and thus it has better spectral efficiency than conventional MIMO. For the double-sided, the null subcarriers are replaced by pilot symbols, and therefore its spectral efficiency is similar to conventional MIMO.

Fig. 6 shows the BER of a MIMO communications link over a flat fading channel using MMSEE and ZFE with single and double-sided pilot configurations where the pilot power boosting factor $\beta = 0$. As can be seen from the figure, the proposed system with double-sided pilot configuration offers a substantial BER improvement over the ZFE and MMSEE with linear and spline channel estimation for the considered signal-to-noise ratios (SNRs) range. Moreover, it outperforms the ZFE with perfect channel estimates when the SNR is

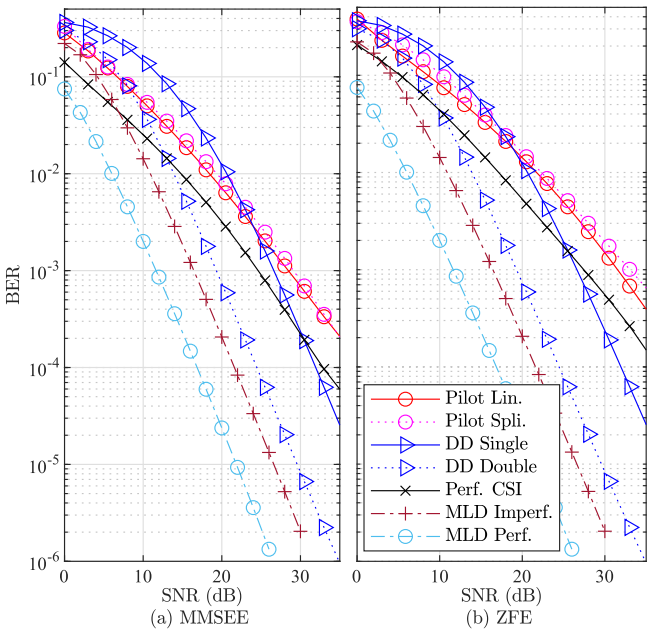

FIGURE 6. BER performance over the flat fading channel using ZFE and MMSEE, with pilot power boost factor $\beta = 0$ dB.

greater than 10 dB. The advantage of the DD with double-sided pilot referencing is also observed over the ZFE even for the case of perfect CSI where a gain of about 13 dB is obtained at BER of 10^{-3}. The figure also presents the BER of the MLD with perfect and imperfect CSI. Although it is mathematically intractable to evaluate the diversity gain of the DD, it can be noted that its BER has roughly the same slope as the MLD, which implies that it has a similar diversity order that is equal to 2. However, the MLD with perfect CSI offers also an 8 dB processing gain advantage over the DD. Nevertheless, the processing gain of the MLD drops to about 3 dB when the MLD is evaluated with imperfect CSI. For the single-sided pilot case, the spectral efficiency gain comes at the cost of BER degradation of about 7.4 dB as compared to the double-sided pilot case. Nevertheless, a significant advantage can still be achieved as compared to the conventional ZFE with linear and spline interpolation at moderate and high SNRs. The same observations are generally applicable to the MMSEE in Fig. 6(b). As expected, the minimum mean square error (MMSE) BER improves by 3 dB for the perfect CSI case, however, this is achieved while assuming an ideal estimation of the AWGN power. Therefore, the proposed scheme maintains its BER advantage under the same spectral efficiency conditions.

Fig. 7 shows the BER of a MIMO system over a flat fading channel using MMSEE and ZFE with single and double-sided pilots and using $\beta = 3$ dB, which represents the pilot power boost. The higher value of β improves system performance compared to the case where $\beta = 0$. As the figure indicates, the proposed DD scheme achieves BER performance that is roughly equal to the MLD with imperfect CSI and approximately 3 dB away from the optimal MLD with perfect CSI.

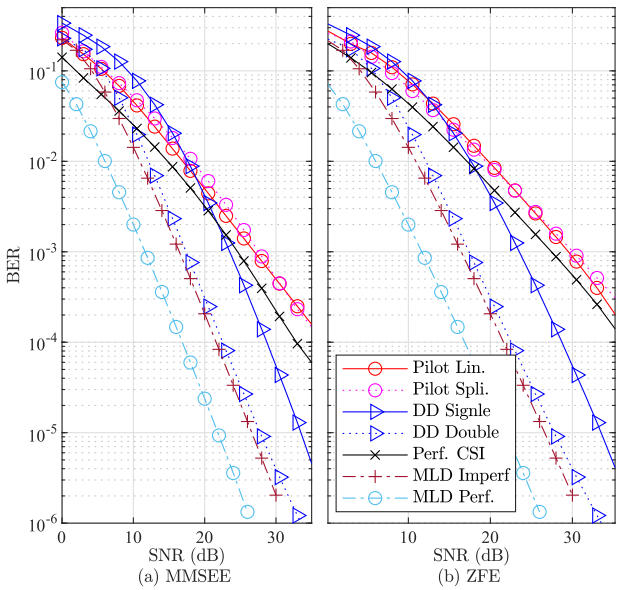

FIGURE 7. BER performance over the flat fading channel using ZFE and MMSEE equalizers, $\beta = 3$ dB.

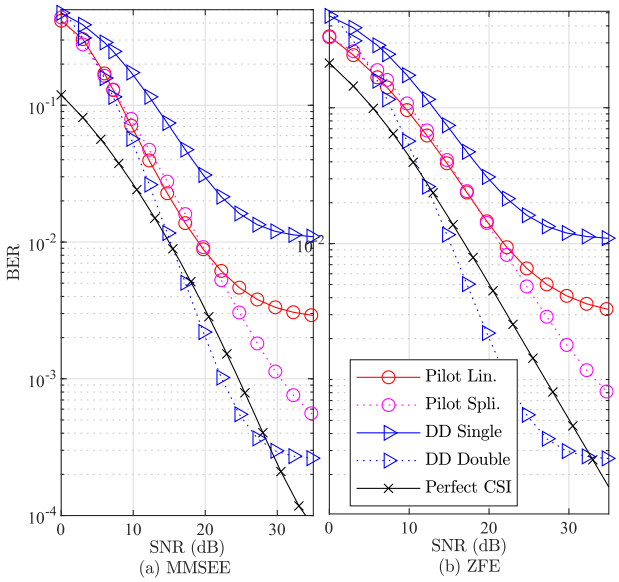

FIGURE 8. BER performance over the FS fading channel using ZFE and MMSEE, $\beta = 0$ dB.

The pilot power boosting demonstrated a more significant impact on the DD as compared to other schemes, which is manifested in terms of BER improvement.

Fig. 8 is generated for the DD, ZFE, and MMSEE with single and double-sided pilots where $\beta = 0$ dB. The channel considered channel is FS. Generally speaking, the same trends observed for the flat channel are observed for the FS fading case. However, all considered systems suffer from error floors due to the severe fading inherent to the selectivity of the channel, which causes more channel estimation errors for the ZFE and MMSE. For the DD, the fading of the pilots may cause detection ambiguity, which can increase the BER.

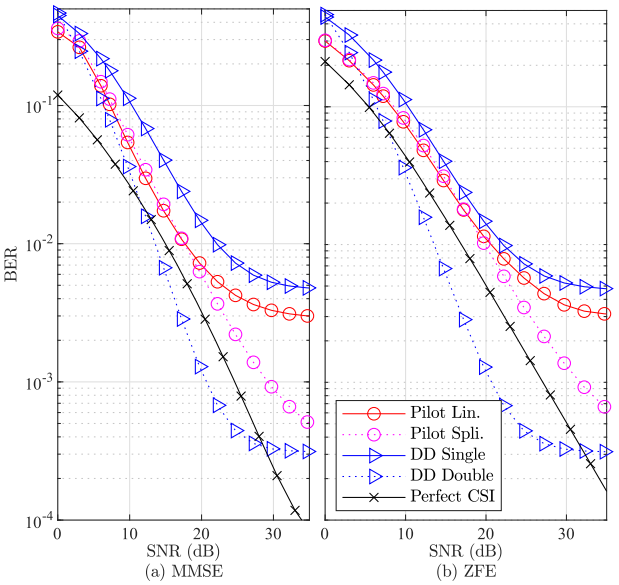

FIGURE 9. BER performance over the FS fading channel using ZFE and MMSEE, $\beta = 3$ dB.

Moreover, since the system is implemented in the frequency domain, the channel fading over multiple adjacent subcarriers will be slightly different, which implies that the channel equality assumption will be violated. Nevertheless, the DD performance remains superior for various configurations and channel conditions for moderate and high SNRs.

Fig. 9 is similar to Fig. 8 except that $\beta = 3$ dB. As the figure shows, the 3 dB pilot boost managed to improve the BER for medium and high SNRs, but did not reduce the error floor for the double-sided DD scheme. Such performance is obtained because the error floor for the double-sided DD mostly depends on the frequency selectivity of the channel. On the contrary, the effect of imperfect channel state information CSI on conventional techniques MMSE and ZFE is negligible at high SNRs.

V. CONCLUSIONS AND FUTURE WORK

This work presented a novel low complexity scheme that can allow deploying MIMO technology in small IoT, WSN nodes, and UAVs. The new system does not require knowledge of the channel information as in the case of conventional MIMO systems, making it a strong candidate for future URLLC IoT services. Moreover, it offers substantial BER and spectral efficiency improvement over existing systems. The BER improvement is gained because the system offers near-MLD performance with reasonable processing complexity. In particular scenarios, the gain obtained by the proposed system can be as high as 15 dB in terms of BER and 16.6% in terms of spectral efficiency. The system complexity is considered low as well because it does not require the channel matrix inversion process at the receiver side, which can be prohibitively complex for IoT nodes with limited computational capabilities.

In future work, we will consider performing a thorough performance analysis to obtain deep insights into the system performance under various operating conditions. Moreover, more results will be included using a larger number of antennas, multiple users, more pilot designs and boosting scenarios. Moreover, it would be insightful to develop a testbed to evaluate the performance of the proposed system under various channel and system conditions.

REFERENCES

[1] J. v. Mankowski, E. Durmaz, A. Papa, H. Vijayaraghavan, and W. Kellerer, "Aerial-aided multiaccess edge computing: Dynamic and joint optimization of task and service placement and routing in multilayer networks," *IEEE Trans. Aerosp. Electron. Syst.*, vol. 59, no. 3, pp. 2593–2607, Jun. 2023.

[2] "Minimum requirements related to technical performance for IMT-2020 radio interface(s)" International Communications Union (ITU), Geneva, Switzerland, Tech. Rep. ITU-R M.2410-0, Nov. 2017. [Online]. Available: https://www.itu.int/dms_pub/itu-r/opb/rep/R-REP-M.2410-2017-PDF-E.pdf

[3] H. Huang, A. V. Savkin, and C. Huang, "Decentralized autonomous navigation of a UAV network for road traffic monitoring," *IEEE Trans. Aerosp. Electron. Syst.*, vol. 57, no. 4, pp. 2558–2564, Aug. 2021.

[4] A. Giorgetti, M. Lucchi, M. Chiani, and M. Z. Win, "Throughput per pass for data aggregation from a wireless sensor network via a UAV," *IEEE Trans. Aerosp. Electron. Syst.*, vol. 47, no. 4, pp. 2610–2626, Oct. 2011.

[5] M. Thammawichai, S. P. Baliyarasimhuni, E. C. Kerrigan, and J. B. Sousa, "Optimizing communication and computation for multi-UAV information gathering applications," *IEEE Trans. Aerosp. Electron. Syst.*, vol. 54, no. 2, pp. 601–615, Apr. 2018.

[6] M. A. Al-Jarrah, M. A. Yaseen, A. Al-Dweik, O. A. Dobre, and E. Alsusa, "Decision fusion for IoT-based wireless sensor networks," *IEEE Internet Things J.*, vol. 7, no. 2, pp. 1313–1326, Feb. 2020.

[7] M. A. Al-Jarrah, A. Al-Dweik, M. Kalil, and S. S. Ikki, "Decision fusion in distributed cooperative wireless sensor networks," *IEEE Trans. Veh. Technol.*, vol. 68, no. 1, pp. 797–811, Jan. 2019.

[8] M. A. Albreem, M. Juntti, and S. Shahabuddin, "Massive MIMO detection techniques: A survey," *IEEE Commun. Surv. Tuts.*, vol. 21, no. 4, pp. 3109–3132, Fourthquarter 2019.

[9] Y. Iraqi and A. Al-Dweik, "Efficient information transmission using smart OFDM for IoT applications," *IEEE Internet Things J.*, vol. 7, no. 9, pp. 8397–8409, Sep. 2020.

[10] X. Wu, X. Yang, S. Ma, B. Zhou, and G. Yang, "Hybrid channel estimation for UPA-assisted millimeter-wave massive MIMO IoT systems," *IEEE Internet Things J.*, vol. 9, no. 4, pp. 2829–2842, Feb. 2022.

[11] O. Cetinkaya, D. Balsamo, and G. V. Merrett, "Internet of MIMO Things: UAV-assisted wireless-powered networks for future smart cities," *IEEE Internet Things Mag.*, vol. 3, no. 1, pp. 8–13, Mar. 2020.

[12] M. Al-Jarrah, E. Alsusa, A. Al-Dweik, and M. Alouini, "Performance analysis of wireless mesh backhauling using intelligent reflecting surfaces," *IEEE Trans. Wireless Commun.*, vol. 20, no. 6, pp. 3597–3610, Jun. 2021.

[13] H. Huang, C. Papadias, and S. Venkatesan, *MIMO Communication for Cellular Networks*. New York, NY, USA: Springer Publishing Company, Incorporated, 2011.

[14] R. Zhang, W. Hao, G. Sun, and S. Yang, "Hybrid precoding design for wideband THz massive MIMO-OFDM systems with beam squint," *IEEE Syst. J.*, vol. 15, no. 3, pp. 3925–3928, Sep. 2021.

[15] B. Shi et al., "Impact of low-resolution ADC on DOA estimation performance for massive MIMO receive array," *IEEE Syst. J.*, vol. 16, no. 2, pp. 2635–2638, Jun. 2022.

[16] S. Wang, M. He, R. Ruby, and Y. Zhang, "SVM-based optimization on the number of data streams for massive MIMO systems," *IEEE Syst. J.*, vol. 17, no. 1, pp. 83–86, Mar. 2023.

[17] N. Fatema, G. Hua, Y. Xiang, D. Peng, and I. Natgunanathan, "Massive MIMO linear precoding: A survey," *IEEE Syst. J.*, vol. 12, no. 4, pp. 3920–3931, Dec. 2018.

[18] G. Liu, H. Deng, X. Qian, W. Zhang, and H. Dong, "Joint pilot and data power control for cell-free massive MIMO IoT systems," *IEEE Sensors J.*, vol. 22, no. 24, pp. 24647–24657, Dec. 2022.

[19] L. Chen, B. Hu, G. Xu, and S. Chen, "Energy-efficient power allocation and splitting for mmWave beamspace MIMO-NOMA with SWIPT," *IEEE Sensors J.*, vol. 21, no. 14, pp. 16381–16394, Jul. 2021.

[20] The LoRa Alliance, "Lorawan certified devices," 2023. [Online]. Available: https://lora-alliance.org/lora_products/lsn50v2/

[21] "Low SWaP integrated radio system for UAS, UGV, and USV." Accessed: Oct. 01, 2023. [Online]. Available: https://www.unmannedsystemstechnology.com/company/triad-rf-systems/thpr1009-d03-high-power-radio/

[22] "915mhz 3dr radio telemetry module 40 km data link pixhawk." Accessed: Oct. 01, 2023. [Online]. Available: https://brushlessgimbal.ca/Auto-Pilot-Flight-Controller/915Mhz-3DR-Radio-Telemetry-Module-40KM-Data-Link-Pixhawk

[23] "Streamcaster 4400 enhanced 4 × 4 MIMO radio." Accessed: Oct. 01, 2023. [Online]. Available: https://silvustechnologies.com/wp-content/uploads/2023/09/StreamCaster-4400-SC4400E-Enhanced-Datasheet-1.pdf

[24] B. Hochwald and S. t. Brink, "Achieving near-capacity on a multiple-antenna channel," *IEEE Trans. Commun.*, vol. 51, no. 3, pp. 389–399, Mar. 2003.

[25] B. Hassibi and H. Vikalo, "On the sphere-decoding algorithm I. Expected complexity," *IEEE Trans. Signal Process.*, vol. 53, no. 8, pp. 2806–2818, Aug. 2005.

[26] C. Studer and H. Bölcskei, "Soft–input soft-output single tree-search sphere decoding," *IEEE Trans. Inf. Theory*, vol. 56, no. 10, pp. 4827–4842, Oct. 2010.

[27] C. Studer, A. Burg, and H. Bolcskei, "Soft-output sphere decoding: Algorithms and VLSI implementation," *IEEE J. Sel. Areas Commun.*, vol. 26, no. 2, pp. 290–300, Feb. 2008.

[28] J. C. Hedstrom, C. H. Yuen, R.-R. Chen, and B. Farhang-Boroujeny, "Achieving near map performance with an excited Markov chain Monte Carlo MIMO detector," *IEEE Trans. Wireless Commun.*, vol. 16, no. 12, pp. 7718–7732, Dec. 2017.

[29] R.-r. Chen, R. Peng, A. Ashikhmin, and B. Farhang-Boroujeny, "Approaching MIMO capacity using bitwise Markov chain Monte Carlo detection," *IEEE Trans. Commun.*, vol. 58, no. 2, pp. 423–428, Feb. 2010.

[30] J. C. Hedstrom, A. Rezazadehreyhani, C. H. Yuen, and B. Farhang-Boroujeny, "A capacity achieving MIMO detector based on stochastic sampling," *IEEE Open J. Commun. Soc.*, vol. 2, pp. 2436–2448, 2021.

[31] R. Peng, K. H. Teo, J. Zhang, and R.-R. Chen, "Low-complexity hybrid QRD-MCMC MIMO detection," in *Proc. IEEE Glob. Telecommun. Conf.*, 2008, pp. 1–5.

[32] R.-H. Peng, R.-R. Chen, and B. Farhang-Boroujeny, "Markov chain Monte Carlo detectors for channels with intersymbol interference," *IEEE Trans. Signal Process.*, vol. 58, no. 4, pp. 2206–2217, Apr. 2010.

[33] B. Hassibi, M. Hansen, A. G. Dimakis, H. A. J. Alshamary, and W. Xu, "Optimized Markov chain Monte Carlo for signal detection in MIMO systems: An analysis of the stationary distribution and mixing time," *IEEE Trans. Signal Process.*, vol. 62, no. 17, pp. 4436–4450, Sep. 2014.

[34] S. A. Laraway and B. Farhang-Boroujeny, "Implementation of a Markov chain Monte Carlo based multiuser/MIMO detector," *IEEE Trans. Circuits Syst. I: Regular Papers*, vol. 56, no. 1, pp. 246–255, Jan. 2009.

[35] D. Auras, U. Deidersen, R. Leupers, and G. Ascheid, "VLSI design of a parallel MCMC-based MIMO detector with multiplier-free Gibbs Samplers," in *Proc. 22nd Int. Conf. Very Large Scale Integration*, 2014, pp. 1–6.

[36] J. Chen, J. Hu, and G. E. Sobelman, "Stochastic iterative MIMO detection system: Algorithm and hardware design," *IEEE Trans. Circuits Syst. I: Regular Papers*, vol. 62, no. 4, pp. 1205–1214, Apr. 2015.

[37] Y. Hama and H. Ochiai, "Performance analysis of matched-filter detector for MIMO spatial multiplexing over Rayleigh fading channels with imperfect channel estimation," *IEEE Trans. Commun.*, vol. 67, no. 5, pp. 3220–3233, May 2019.

[38] L. Zheng, C. Yang, X. Deng, and W. Ge, "Linearized model for MIMO-MFSK systems with energy detection," *IEEE Commun. Lett.*, vol. 26, no. 6, pp. 1408–1412, Jun. 2022.

[39] A. Saci, A. Al-Dweik, and A. Shami, "Direct data detection of OFDM signals over wireless channels," *IEEE Trans. Veh. Technol.*, vol. 69, no. 11, pp. 12432–12448, Nov. 2020.

[40] 3rd Generation Partnership Project (3GPP), "LTE; evolved universal terrestrial radio access (E-UTRA); physical channels and modulation," 3GPP, Technical Specification (TS) 36.211, 2011, version 10.0.0. [Online]. Available: https://portal.3gpp.org/desktopmodules/Specifications/SpecificationDetails.aspx?specificationId=2440
[41] E. Dahlman, S. Parkvall, J. Sköld, and P. Beming, *3 G Evolution : HSPA and LTE for Mobile Broadband*, 2nd ed. New York, NY, USA: Elsevier, 2007.
[42] A. Saci, A. Al-Dweik, A. Shami, and Y. Iraqi, "One-shot blind channel estimation for OFDM systems over frequency-selective fading channels," *IEEE Trans. Commun.*, vol. 65, no. 12, pp. 5445–5458, Dec. 2017.
[43] M. Mozaffari, W. Saad, M. Bennis, and M. Debbah, "Wireless communication using unmanned aerial vehicles (UAVs): Optimal transport theory for hover time optimization," *IEEE Trans. Wireless Commun.*, vol. 16, no. 12, pp. 8052–8066, Dec. 2017.
[44] A. A. Khuwaja, Y. Chen, N. Zhao, M.-S. Alouini, and P. Dobbins, "A survey of channel modeling for UAV communications," *IEEE Commun. Surv. Tut.*, vol. 20, no. 4, pp. 2804–2821, Fourthquarter 2018.
[45] G. J. Byers and F. Takawira, "Spatially and temporally correlated MIMO channels: Modeling and capacity analysis," *IEEE Trans. Veh. Technol.*, vol. 53, no. 3, pp. 634–643, May 2004.
[46] A. Al-Dweik, F. Kalbat, S. Muhaidat, O. Filio, and S. M. Ali, "Robust MIMO-OFDM system for frequency-selective mobile wireless channels," *IEEE Trans. Veh. Technol.*, vol. 64, no. 5, pp. 1739–1749, May 2015.
[47] J. R. Hampton, *Introduction to MIMO Communications*. Cambridge, U.K.: Cambridge Univ. Press, 2013.
[48] R. K. Ganti and M. Haenggi, "Spatial and temporal correlation of the interference in ALOHA ad hoc networks," *IEEE Commun. Lett.*, vol. 13, no. 9, pp. 631–633, Sep. 2009.
[49] S. An, Q. Zhu, J. Li, Y. Ling, and Y. Su, "112-Gb/s SSB 16-QAM signal transmission over 120-km SMF with direct detection using a MIMO-ANN nonlinear equalizer," *Opt. Exp.*, vol. 27, no. 9, pp. 12794–12805, Apr. 2019. [Online]. Available: https://opg.optica.org/oe/abstract.cfm?URI=oe-27-9-12794
[50] H. Kato, T. H. Tran, and Y. Nakashima, "ASIC design of a low-complexity K-best Viterbi decoder for IoT applications," in *Proc. IEEE Asia Pacific Conf. Circuits Syst.*, 2016, pp. 396–399.
[51] Z.-Y. Wang and P.-Y. Tsai, "Design and implementation of a 6.5-Gb/s multiradix simplified viterbi-sphere decoder for trellis-coded generalized spatial modulation with spatial multiplexing," *IEEE Trans. Very Large Scale Integr. VLSI Syst.*, vol. 30, no. 12, pp. 1853–1866, Dec. 2022.

ANAS SACI (Member, IEEE) received the B.Sc. degree from the Jordan University of Science and Technology, Irbid, Jordan, in 2013, and the M.Sc. degree from Télécom ParisTech, France, in 2015, and the Ph.D. degree in electrical and computer engineering from the University of Western Ontario, London, ON, Canada, in 2020. His research interests include wireless communications, digital signal processing, machine learning, and statistical modeling.

ARAFAT AL-DWEIK (Senior Member, IEEE) received the M.S. (*summa cum laude*) and Ph.D. (*magna cum laude*) degrees in electrical engineering from Cleveland State University, Cleveland, OH, USA, in 1998 and 2001, respectively. He was with Efficient Channel Coding Inc., Cleveland, the Department of Information Technology, Arab American University, Jenin, Palestine, and the University of Guelph, Guelph, ON, Canada. He is currently with the Department of Electrical Engineering and Computer Science, Khalifa University, Abu Dhabi, United Arab Emirates. He is also a Visiting Research Fellow with the School of Electrical, Electronic, and Computer Engineering, Newcastle University, Newcastle upon Tyne, U.K., and a Research Professor with Western University, London, ON, Canada, and the University of Guelph. He has extensive research experience in various areas of wireless communications that include modulation techniques, channel modeling and characterization, synchronization and channel estimation techniques, OFDM technology, error detection and correction techniques, MIMO, and resource allocation for wireless networks. He is a member of Tau Beta Pi and Eta Kappa Nu. He was the recipient of the UAE Lead-er-Founder Award, in 2019, the Dubai Award for Sustainable Transportation, in 2016, the Hijjawi Award for Applied Sciences, in 2003, and the Fulbright Alumni Development Grant, in 2003 and 2005. He was awarded the Fulbright Graduate Student Scholarship, from 1997 to 1999. Since 2012, he has been the Editor of IEEE TRANSACTIONS ON VEHICULAR TECHNOLOGY. He was an Associate Editor for the *IET Communications*, from 2015 to 2020, and Frontiers in Communications and Networks, since 2021. He is a registered Professional Engineer in the Province of Ontario, Canada. He is a Distinguished Lecturer of the IEEE (2023–2025).

SHIHAB JIMAA (Senior Member, IEEE) received the M.Sc. and Ph.D. degrees in digital communications from Loughborough University, England, U.K., in 1986 and 1990, respectively. He received a Post Graduate Certificate in Higher Education (PGCE) from the University of Hertfordshire, U.K. in 1998. He is currently an Associate Professor with the Khalifa University of Science and Technology, Abu Dhabi, United Arab Emirates. He has authored three book chapters, one patent, and about 100 papers in various referred inter-national conferences and journals. His research interests include wireless communication systems and networks, channel estimation and equalization, and signal processing for digital communications/Biomedical engineering. Dr. Jimaa is a U.K. Chartered Electrical Engineer, a Senior Member of the IEEE Communications and Education societies, a member of IET, and a fellow member of the Higher Education Academy (HEA)/U.K. He is the Guest Editor of the Special Issue on Energy Efficient Wireless Communication Networks with QoS, International Journal of Communication Systems by John Wiley, 2017.